Enhancement of Ni–$(Y_2O_3)_{0.08}(ZrO_2)_{0.92}$ fuel electrode performance by infiltration of $Ce_{0.8}Gd_{0.2}O_{2-\delta}$ nanoparticles

Beom-Kyeong Park, Roberto Scipioni, Dalton Cox, and Scott A. Barnett *

Department of Materials Science and Engineering, Northwestern University, Evanston, Illinois 60208, USA

*** Corresponding author**

E-mail: s-barnett@northwestern.edu

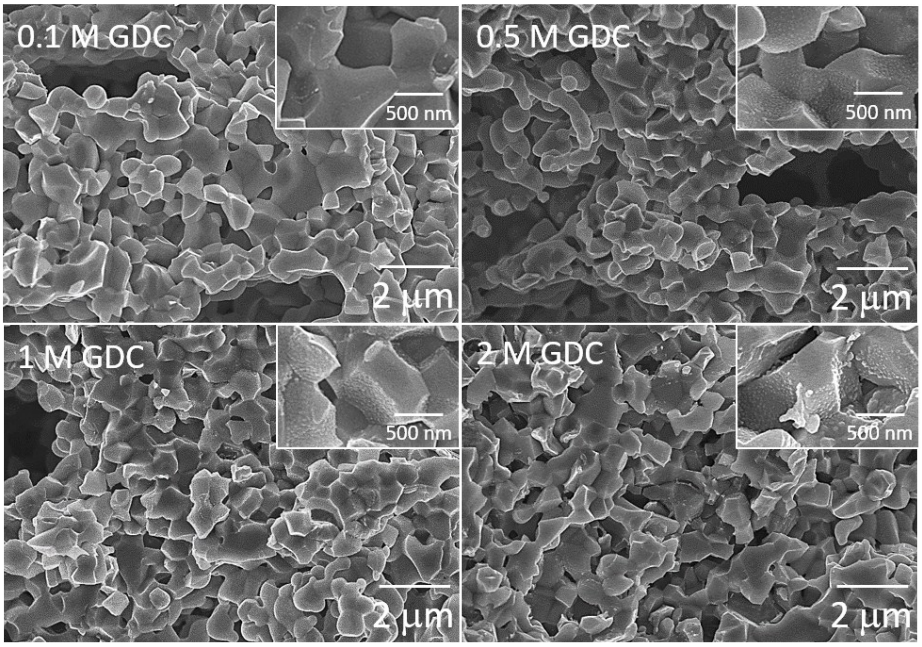

Fig. S1 Cross-sectional SEM images of the surface-modified Ni–YSZ supports (after electrochemical characterization): pristine; (single-step) infiltration of 0.1 M GDC; infiltration of 0.5 M GDC; infiltration of 1 M GDC; and infiltration of 2 M GDC.

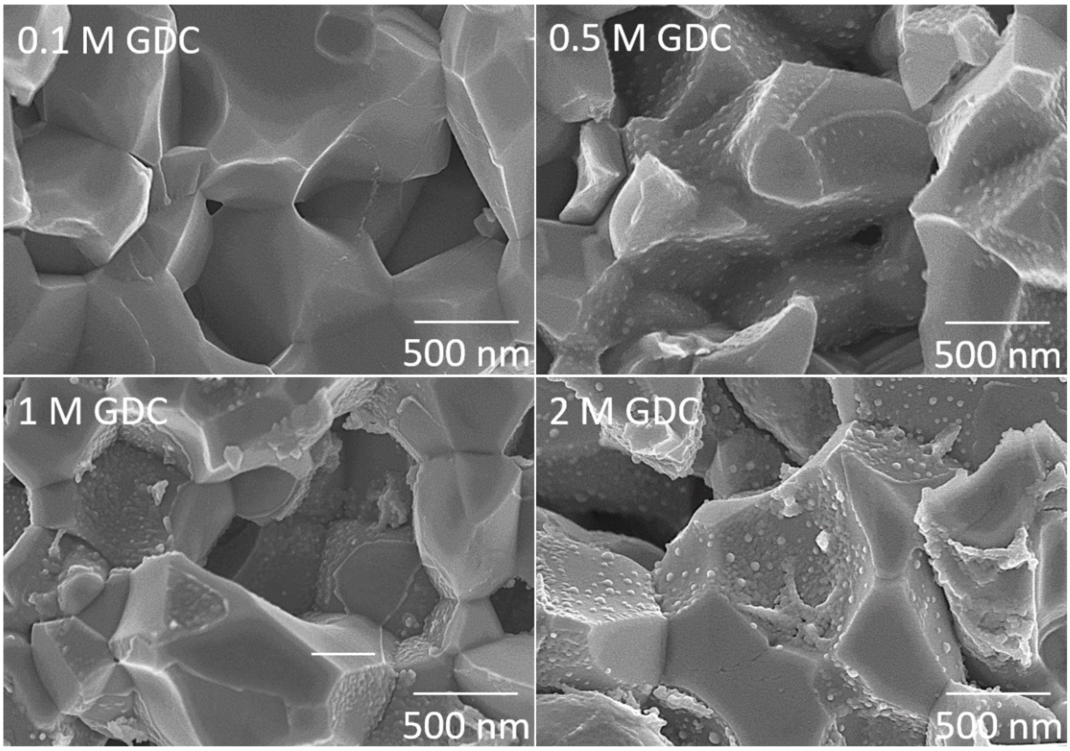

Fig. S2 Cross-sectional SEM images of surface-modified Ni–YSZ electrodes of the electrolyte-supported symmetric cells (after electrochemical characterization): pristine; (single-step) infiltration of 0.1 M GDC; infiltration of 0.5 M GDC; infiltration of 1 M GDC; and infiltration of 2 M GDC.

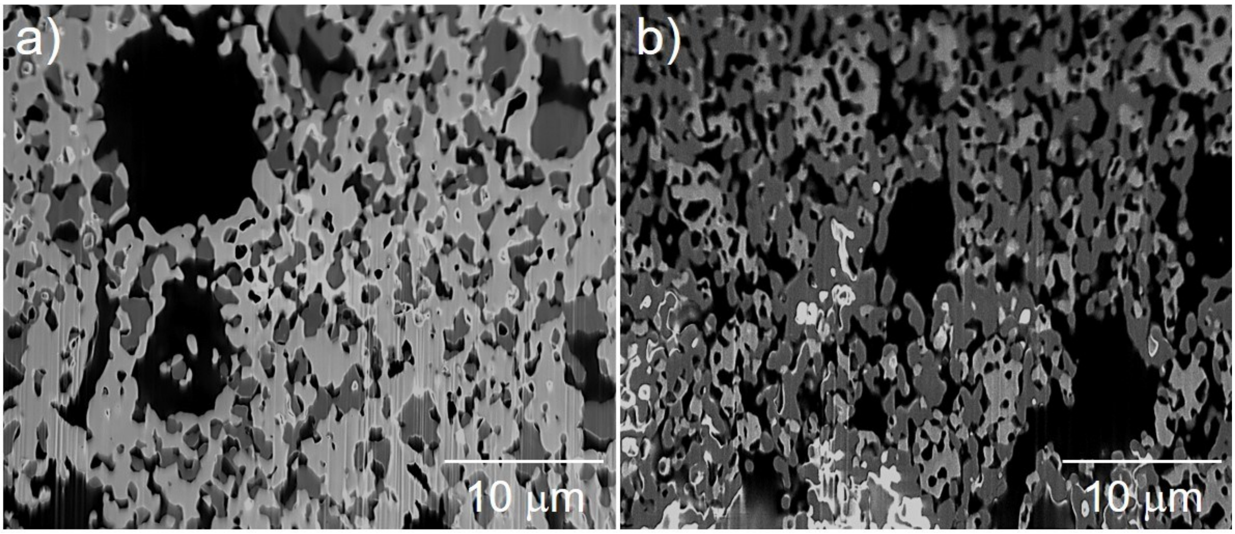

Fig. S3 Polished cross-sectional SEM images of the fuel-electrode support layers (FESLs) of (a) Ni–YSZ supported symmetric cell (FESC) with standard supports (ε = ~0.35) and (b) Ni–YSZ supported full cell with a tailored support (ε = ~0.55) after electrochemical characterization.

The sample was polished up to a 1 μm polishing solution on the top and imaging sides, then a high current Ga beam was used to rough cut the surface, leaving behind the curtaining. A low current beam was then applied as a cleaning cut to remove the large curtaining. While the black color indicates the pore, the bright and dark gray colors indicate the Ni and YSZ, respectively.

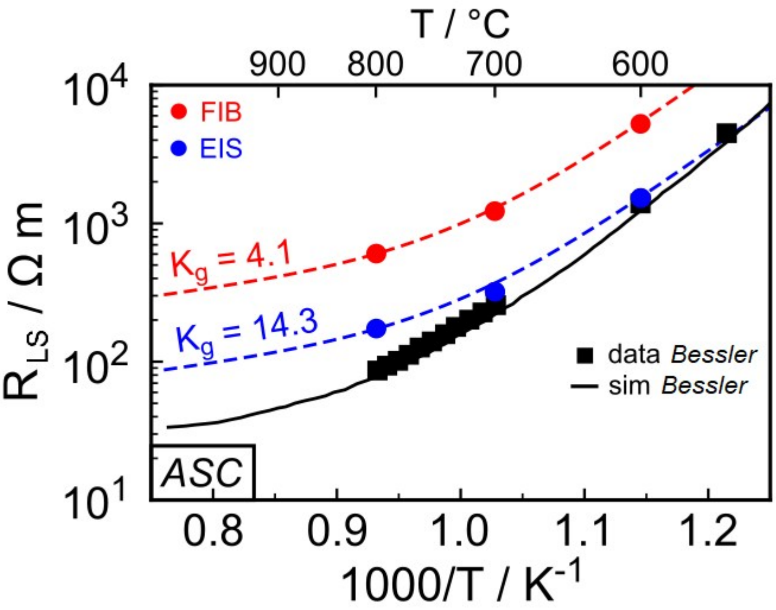

Fig. S4 TPB line-specific resistance (R_{LS}) values calculated for the fuel-electrode-supported cell without GDC infiltration. The resultant data are compared with the data from the literature.

A quantitative test of the present EIS data was made by determining the TPB line-specific resistance (R_{LS}) using a modified form of eq. 1 (in the manuscript) that gives the TLM portion of the EIS response $R_{P,TLM}$:[1]

$$R_{P,TLM} = \sqrt{\frac{R_{LS}}{l_{TPB}\sigma_{ion}/K_g}}\coth\left(L\sqrt{\frac{l_{TPB}}{R_{LS}\,\sigma_{ion}/K_g}}\right),$$

where l_{TPB} is the active TPB density of ~7.2 μm^{-2}, as previously measured by 3D tomography of a similar electrode and σ_{ion} is YSZ ionic conductivity normalized by a geometrical factor K_g, defined as the ratio between YSZ tortuosity and volume fraction (τ_{YSZ}/φ_{YSZ}).[2] This value is obtained either by FIB tomography,[2] or from the $R_{O^{2-}}$ value obtained by EIS fitting using the relation:[3]

$$\tau_{YSZ} = \varphi_{YSZ}\,\sigma_{ion}\,R_{O^{2-}}$$

Fig. S4 shows the R_{LS} for the electrode with no GDC infiltration at different temperature, normalized to the geometrical factors calculated by FIB tomography and EIS fitting. The curves are compared with the data and simulation reported by Bessler *et. al.*.[1] Although K_{g} calculated by EIS fitting (K_{g}=14.3) is ~3.5 times higher than the effective one measured by FIB tomography (K_{g}=4.1), the EIS-based R_{LS} data (blue dashed line) shows a better agreement with the reported literature values (black line).[1,2] The data reported by Bessler *et.al.* were extracted using the software WebPlotDigitizer.[1,4]

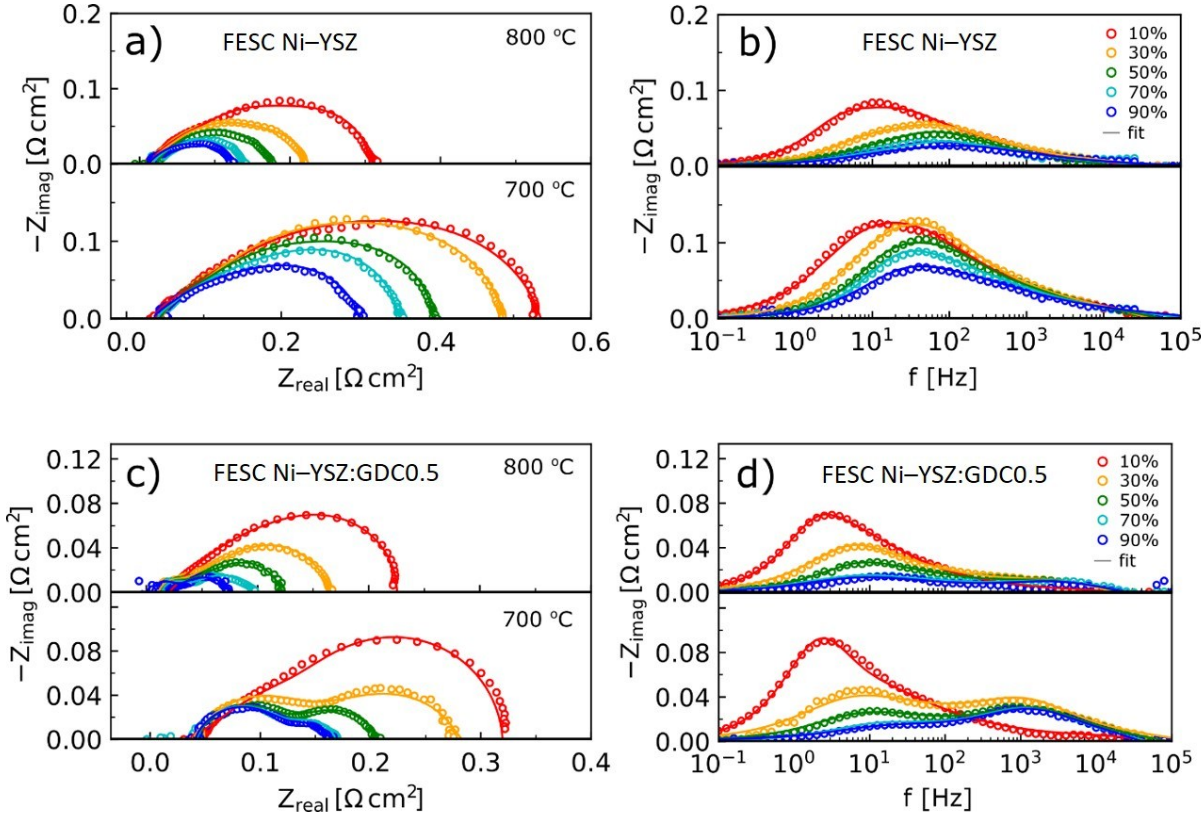

Fig. S5 Nyquist and Bode plots of the selected impedance spectra for FESCs with (a,b) Ni–YSZ and (c,d) Ni–YSZ:GDC0.5. The measurement was carried out at 700 and 800 °C at increasing the steam content in H_2. All the spectra include the best fits (solid lines) to the data using the equivalent circuit described in Fig. 5.

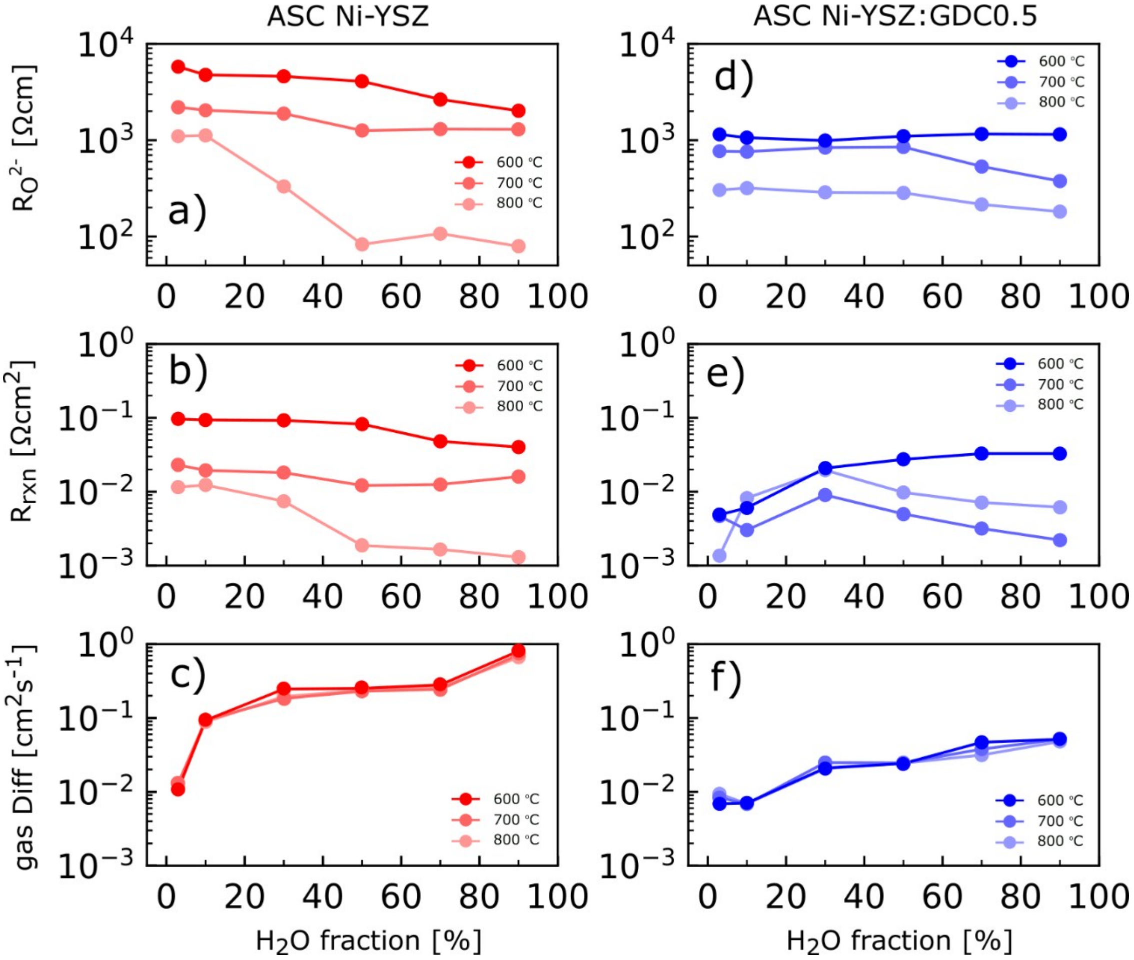

Fig. S6 (a,d) $R_{O^{2-}}$, (b,e) R_{rxn}, and (c,f) D_{gas} values as a function of H_2O fraction for fuel-electrode-supported (a,b,c) Ni–YSZ and (d,e,f) Ni–YSZ:GDC0.5, measured at 600, 700, and 800 °C.

For Ni–YSZ:GDC0.5, $R_{O^{2-}}$ remains constant at 600 °C but decreased with increasing steam at higher temperatures; R_{rxn} at 600 °C increases with increasing steam and the values are similar for the infiltrated and non-infiltrated electrodes at 90 vol.% H_2O. Noting that the catalytic effect of GDC arises from its mixed conductivity in a reducing atmosphere, the increase in R_{rxn} at 600

^{o}C may reflect that GDC becomes less electronically conductive under high steam and low temperature, and in turn loses its catalytic activity. It is less clear for the behaviors of R_{rxn} at 700 and 800 ^{o}C for Ni–YSZ:GDC0.5, such as the recovery of R_{rxn} at higher steam over 30 vol.% and higher R_{rxn} values rather at 800 ^{o}C. The gas diffusivity increases rapidly with increasing steam content for Ni–YSZ, and it is unchanged with temperature, as expected because higher steam contents are required for effective mass transport given the lower inherent diffusivity of H_2O compared to H_2.

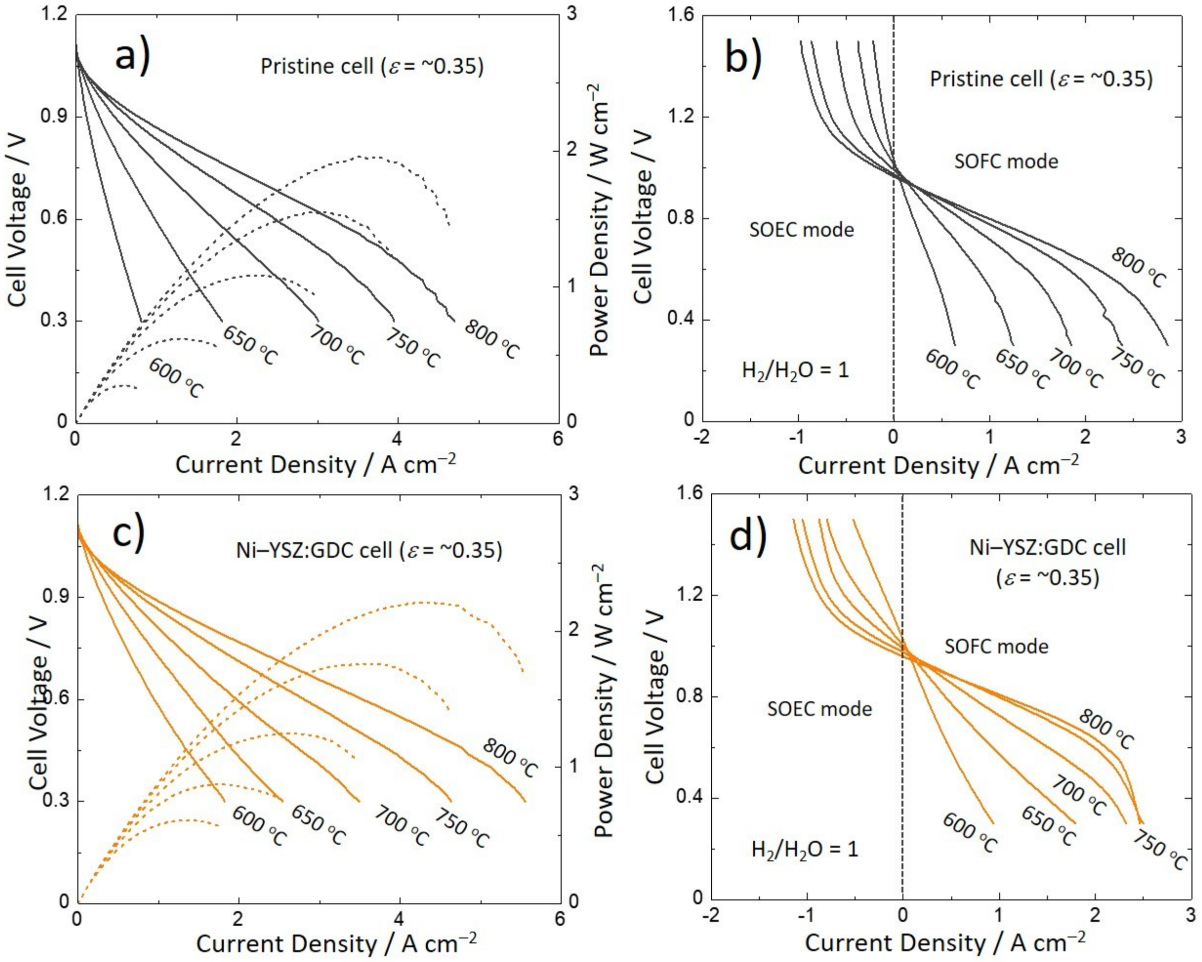

Fig. S7 Electrochemical characteristics of the fuel electrode-supported SOCs (ε = ~0.35) with (a,b) Ni–YSZ and (c,d) Ni–YSZ:GDC0.5 under the typical fuel cell operating condition (3 vol.% H_2O-humidified H_2 and air) and steam electrolysis condition (50 vol.% H_2O-humidified H_2 and air).

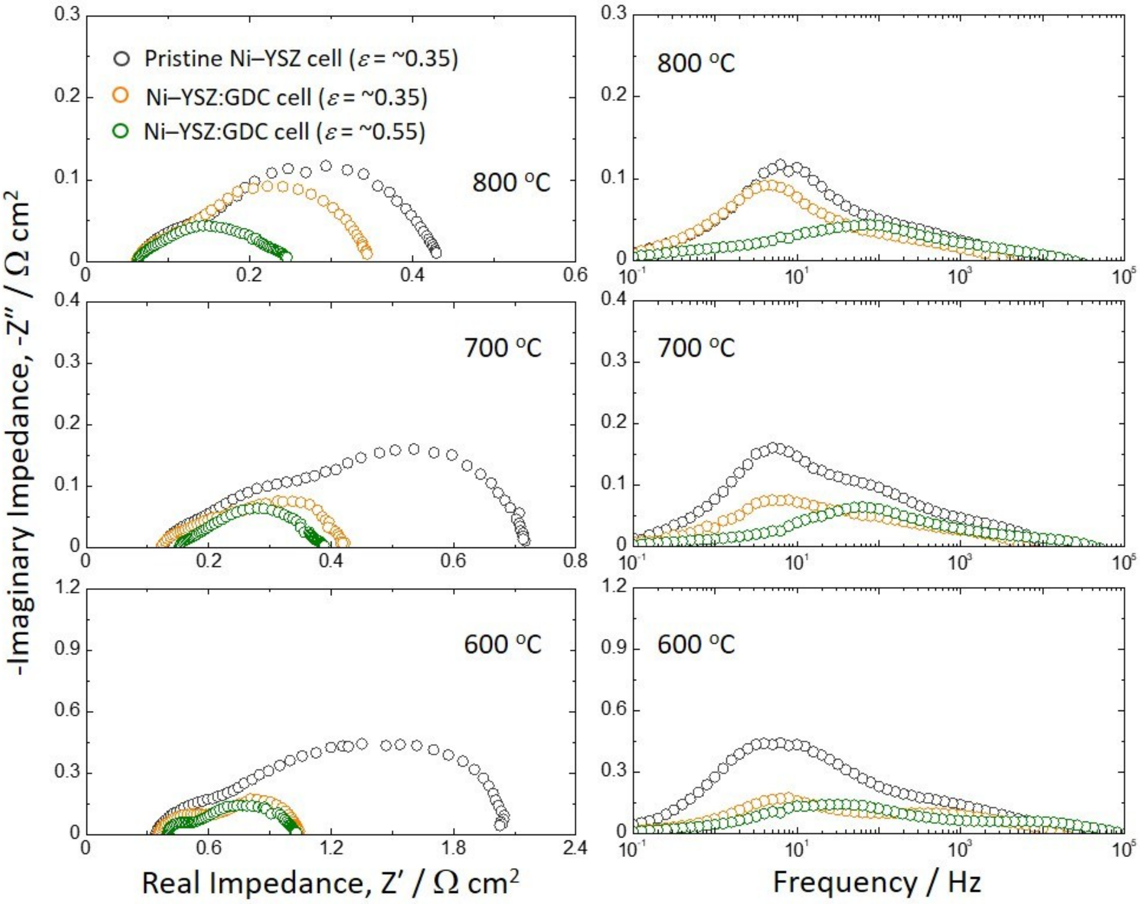

Fig. S8 The comparison of the impedance spectra in the Nyquist and Bode plots for the fuel electrode-supported SOCs with Ni–YSZ (ε = ~0.35) and Ni–YSZ:GDC0.5 (ε = ~0.35 and ~0.55) under the typical fuel cell operating condition (3 vol.% H_2O-humidified H_2 and air).

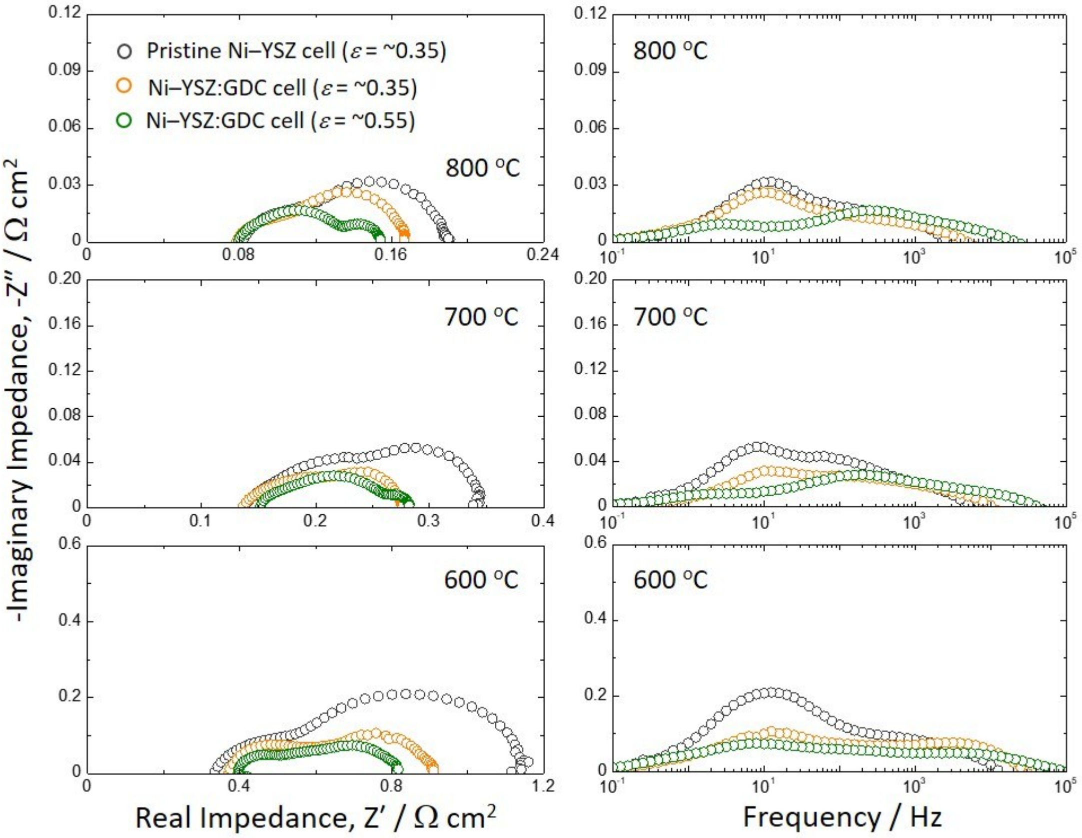

Fig. S9 The comparison of the impedance spectra in the Nyquist and Bode plots for the fuel electrode-supported SOCs with Ni–YSZ (ε = ~0.35) and Ni–YSZ:GDC0.5 (ε = ~0.35 and ~0.55) under the steam electrolysis condition (50 vol.% H_2O-humidified H_2 and air).

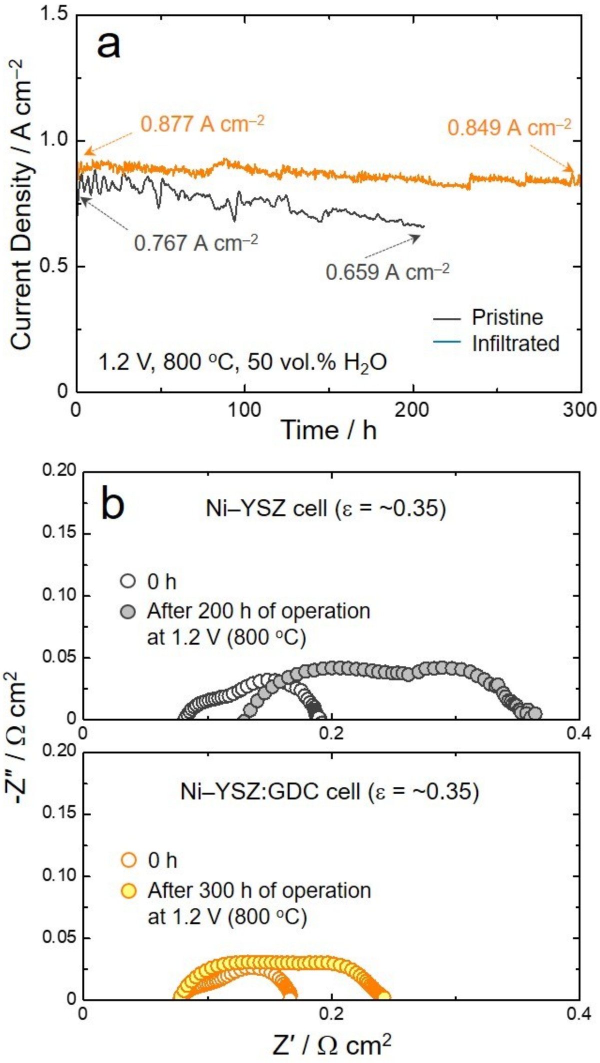

Fig. S10 (a) Current density *vs*. time for the Ni–YSZ and Ni–YSZ:GDC0.5 electrode cells (ε = ~0.35) measured at 1.2 V and 800 °C in 50 vol.% H_2O-humidified H_2 and air. (b) Comparison of impedance spectra in Nyquist plot for the cells in (a) before and after the life tests.

In order to obtain initial results on the effect of GDC infiltration on SOC stability, full cells with and without GDC were electrolysis life tested and the evolution of cell current density with time is presented in Fig. S10(a). Fig. S10(b) also shows the impedance spectra of the cells with Ni–YSZ (ε = ~0.35) and Ni–YSZ:GDC0.5 (ε = ~0.35 and ~0.55) before and after the life tests in 50 vol.% steam. During the life tests at 1.2 V and 800 ^{o}C, the Ni–YSZ:GDC0.5 electrode cell (ε = ~0.35) showed an ~3 % decrease in current density over 300 h, much less than the ~14 % decrease observed over 200 h for the Ni–YSZ electrode cell. The comparison of the EIS data between the cells offers insights into the factors causing the degradation. Along with the increase in R_{Ω}, the Ni–YSZ electrode cell exhibited a relatively high increase in R_{p}. In contrast, the Ni–YSZ:GDC0.5 electrode cell (ε = ~0.35) had a stable R_{Ω} value and a lesser R_{p} increase.

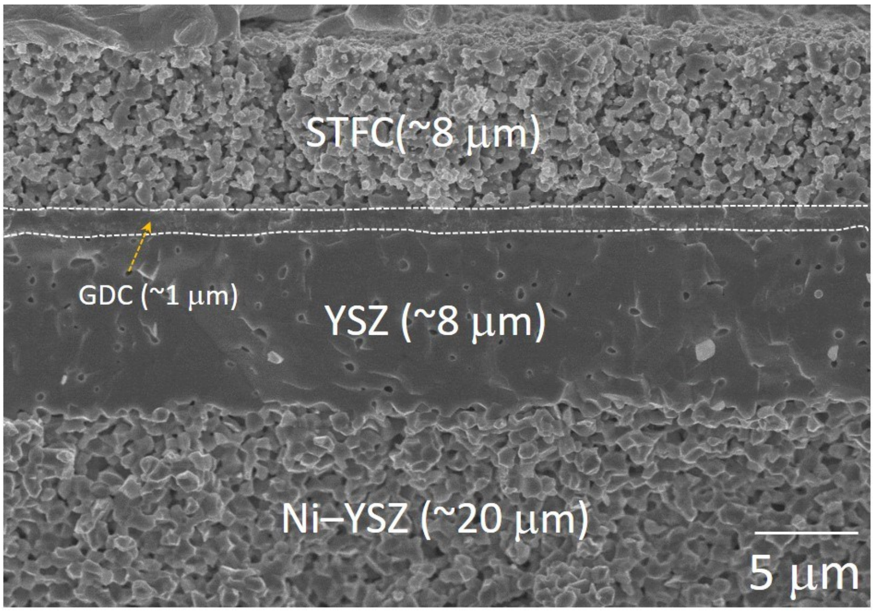

Fig. S11 A cross-sectional SEM image for Ni–YSZ supported SOC with STFC after the polarization (current *vs*. voltage) characterization in fuel cell mode.

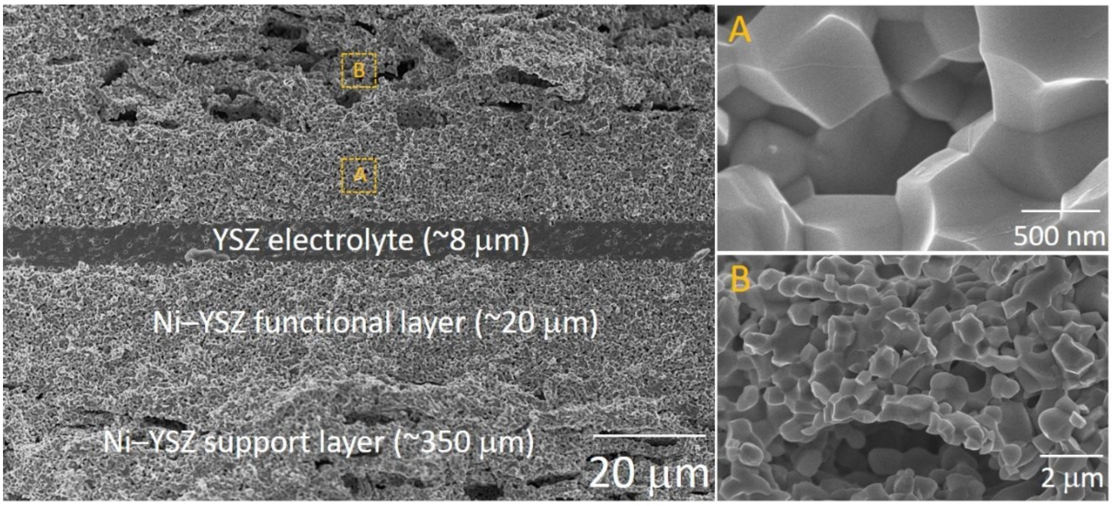

Fig. S12 Cross-sectional SEM images for Ni–YSZ supported symmetric cell after the reduction in 3 vol.% H_2O-humidified H_2 at 700 ^oC for 5 h.

Stereological Analysis

2D stereological analyses of the Ni–YSZ support microstructures were performed to obtain specific surface area and porosity. Polished epoxy-infiltrated samples were milled and imaged at 8000× magnification using an FEI Helios FIB-SEM. Images of the electrode were taken in a manner to avoid biasing the results: there was no overlap in images in the x–y plane and milling depth in the z direction was greater than the largest particle size to ensure independence of the sampled areas.

Using in-house MATLAB code, the SEM images (Figures S5) were binaried into solid and pore phases and the total length of interface of the two phases in each 2D image was calculated. Porosity and specific surface area were estimated using the equations:

$$\varepsilon = \varepsilon_A \qquad \text{(S1)}$$

$$a = (4L_A)/\pi \qquad \text{(S2)}$$

Where ε_A is the 2D porosity of the image and L_A is the interface length divided by the area of the image.[5] Values obtained for each image were averaged within the composition dataset. To verify the method, the stereological calculations were performed on previously obtained full 3D reconstruction datasets. It was found that 10 independent images (no particle overlap between images) of the 300 image datasets was sufficient to ensure that 3D porosity and surface area values fell within the error of stereological measurement.

Reference

1. Bessler, W. G.; Vogler, M.; Störmer, H.; Gerthsen, D.; Utz, A.; Weber, A.; Ivers-Tiffée, E., Model anodes and anode models for understanding the mechanism of hydrogen oxidation in solid oxide fuel cells. *Physical Chemistry Chemical Physics* **2010,** *12* (42), 13888-13903.
2. Gao, Z.; Zenou, V. Y.; Kennouche, D.; Marks, L.; Barnett, S. A., Solid oxide cells with zirconia/ceria Bi-Layer electrolytes fabricated by reduced temperature firing. *Journal of Materials Chemistry A* **2015,** *3* (18), 9955-9964.
3. Scipioni, R.; Jørgensen, P. S.; Graves, C.; Hjelm, J.; Jensen, S. H., A Physically-Based Equivalent Circuit Model for the Impedance of a LiFePO4/Graphite 26650 Cylindrical Cell. *Journal of The Electrochemical Society* **2017,** *164* (9), A2017-A2030.
4. Rohatgi, A., WebPlotDigitizer: Version 3.9 of WebPlotDigitizer (Version v3.9). **2015**.
5. Cruz-Orive, L. M., Unbiased Stereology: Three-Dimensional Measurement in Microscopy. *J Anat* **1999,** *194* (Pt 1), 153-157.